1
2
3
4
5
6
7
8
9
10
11
12
13
14
15
16
17
18
19
20
21
22
23
24
25
26
27
28
29
30
31
32
33
34
35
36
37
38
39
40
41
42
43
44
45
46
47
48
49
50
51
52
53
54
55
56
57
58
59
60

The role of electron induced secondary electron emission from SiO_2 surfaces in capacitively coupled radio frequency plasmas operated at low pressures

B. Horváth[1], M. Daksha[2,3], I. Korolov[1], A. Derzsi[1,2], J. Schulze[2,3]

[1] Institute for Solid State Physics and Optics, Wigner Research Centre for Physics, Hungarian Academy of Sciences, 1121 Budapest, Konkoly Thege Miklós str. 29-33, Hungary

[2] Department of Physics, West Virginia University, Morgantown, WV 26506, USA

[3] Institute of Electrical Engineering and Plasma Technology, Ruhr-University Bochum, 44780 Bochum, Germany

E-mail: derzsi.aranka@wigner.mta.hu

Abstract.
The effects of electron induced secondary electron (SE) emission from SiO_2 electrodes in single-frequency capacitively coupled plasmas (CCPs) are studied by Particle-in-Cell/Monte Carlo Collisions (PIC/MCC) simulations in argon gas at 0.5 Pa for different voltage amplitudes. Unlike conventional simulations, we use a realistic model for the description of electron-surface interactions, which takes into account the elastic reflection and the inelastic backscattering of electrons, as well as the emission of electron induced SEs (δ-electrons). The emission coefficients corresponding to these elementary processes are determined as a function of the electron energy and angle of incidence, taking the properties of the surface into account. Compared to the results obtained by using a simplified model for the electron-surface interaction, widely used in PIC/MCC simulations of CCPs, which includes only elastic electron reflection at a constant probability of 0.2, strongly different electron power absorption and ionization dynamics are observed. We find that ion induced SEs (γ-electrons) emitted at one electrode and accelerated to high energies by the local sheath electric field propagate through the plasma almost collisionlessly and impinge on the opposing sheath within a few nanoseconds. Depending on the instantaneous local sheath voltage these energetic electrons are either reflected by the sheath electric field or they hit the electrode surface, where each γ-electron can generate multiple δ-electrons upon impact. These electron induced SEs are accelerated back into the plasma by the momentary sheath electric field and can again generate δ-electrons at the opposite electrode after propagating through the plasma bulk. Overall, a complex dynamics of γ- and δ-electrons is observed including multiple reflections between the boundary sheaths. At high voltages, the electron induced SE emission is found to strongly affect the plasma density and the ionization dynamics and, thus, it represents an important plasma-surface interaction that should be included in PIC/MCC simulations of CCPs under such conditions.

1. Introduction

Low-pressure capacitively coupled plasmas (CCPs) are basic tools for a variety of plasma processing applications, where the interactions of plasma particles with boundary surfaces are of prime importance [1–3]. Investigations of CCPs by the Particle-in-Cell approach combined with Monte Carlo type treatment of collision processes (PIC/MCC method) have largely improved our understanding of the complex physics of these systems [4–10]. While considerable efforts have been made to describe the gas phase plasma accurately in PIC/MCC models of CCPs (by increasing the number of plasma species and collision processes), a number of simplifications are applied regarding the description of the interaction of plasma particles with the boundary surfaces. For heavy particles, which are in most cases only ions, the assumption of a constant ion induced secondary electron emission coefficient is typical, independent of the incident particle energy and angle, the electrode material and its surface conditions. These simplifying assumptions are critical, since previous investigations revealed a strong sensitivity of a variety of important plasma parameters to the choice of this surface coefficient [11–13]. Recently, important effects of the realistic energy and material dependent description of the secondary electron emission (SEE) induced by heavy particles (including fast neutrals) in PIC/MCC simulations of low-pressure CCPs on the calculated discharge characteristics have been pointed out [14–19]. Regarding the description of the electron-surface interactions in such simulations, perfect absorber surfaces are assumed or a constant probability for the elastic reflection of the electrons is generally set, which is independent of the discharge conditions and properties of the boundary surfaces, while other electron-surface processes, e.g. the emission of secondary electrons (SEs) by electron impact are completely neglected. Attempts to describe the interaction of the electrons with the boundary surfaces in a more realistic way in kinetic simulations of low-pressure CCPs are rarely found [14], although the corresponding energy dependent surface coefficients are known for a variety of materials [20–25].

The SEE due to electron impact represents the basis for the imaging of surfaces and is important for the scanning electron microscope [26]. The electron induced SEE has an important role also in stationary plasma thrusters [27–32]. In these fields a general phenomenological model of the SEE is frequently used [21–25], which assumes that the total yield of SEs due to primary electrons (PEs) bombarding a surface (σ) consists of three components: (i) elastically reflected electrons, (ii) inelastically backscattered electrons, and (iii) electron induced SEs (true SEs, or δ-electrons). Therefore,

$$\sigma = \eta_e + \eta_i + \delta, \tag{1}$$

where η_e is the elastic reflection yield (the number of elastically reflected electrons/the number of PEs), η_i is the inelastic backscattering yield (the number of inelastically backscattered electrons/the number of PEs), and δ is the electron induced SE yield (the number of electron induced SEs/the number of PEs). At high energies (several hundreds of eV), the elastically reflected electrons comprise about 3 % of the emitted

electrons [24]. The inelastically backscattered electrons, which comprise about 7 % of the emitted electrons, are those PEs that penetrated the surface, were scattered from one or more atoms inside the material and lost part of their energy before being scattered out of the surface [24]. About 90 % of the emitted electrons are electron induced SEs, which escape the surface with energies below a few tens of eV [23, 24].

Experimental data for σ as a function of the PE energy, ε, result in curves with similar shape for different surface materials: at low energies of the PEs σ increases rapidly with ε, reaches a maximum value σ_{max} at a PE energy ε_{max}, then slowly decreases towards high PE energies. The peak of σ is explained by the fact that low-energy PEs may have insufficient energy to generate a SE, while PEs with relatively high energies are in contact with surface atoms for too short time to generate SEs [24]. While the general shape of $\sigma(\varepsilon)$ is the same for all surface materials, the σ_{max} and ε_{max} values vary over a wide range: σ_{max} is smaller than 2 for most metals and can reach values higher than 10 for some oxides, while ε_{max} takes values between about 100 eV and 1000 eV depending on the material [23, 33]. The secondary electron yield is influenced by the properties of the surface, as well as the angle of incidence of the PEs: σ_{max} and ε_{max} are significantly increased for oblique impact [33].

In CCPs operated at low pressures and at high voltage amplitudes electrons can reach the boundary surfaces with high energies, e.g. ion induced SEs (γ-electrons) generated at one electrode and accelerated towards the opposite electrode by the local sheath electric field. At low pressure most of these electrons cross the bulk collisionlessly. When they arrive at the opposite sheath, they are either reflected or hit the electrode surface, depending on the instantaneous local sheath voltage. Such discharge conditions are typical in industrial applications such as plasma sputtering, etching, and plasma immersed ion implantation (PIII). Under such conditions, depending on the surface material, more than one SE can be emitted due to electron impact, which is expected to have important effects on the electron power absorption and ionization dynamics. The influence of such δ-electrons on the discharge operation and plasma parameters in low-pressure CCPs for electrode materials with high electron induced SE yields has not been studied yet, despite the fact that such materials (e.g. SiO_2) are frequently used in plasma processing applications.

Therefore, in this work, we study the influence of the electron induced SEs on the plasma density, the electron power absorption, and the ionization dynamics by PIC/MCC simulations in argon gas at a low pressure of 0.5 Pa, for SiO_2 electrodes. In the PIC/MCC simulations we use a realistic model for the description of the electron-surface interaction. This model, which is based on the conventional picture of the SEE, takes the energy and angle of incidence of PEs into account, as well as the surface properties for the determination of the partial emission coefficients of the elastic reflection, inelastic backscattering, and electron induced SEE. The simulations performed by using this model show that the realistic description of the electron-surface interaction has a strong influence on the discharge characteristics at low pressures, especially at high voltage amplitudes, where δ-electrons play a key role in the electron power absorption and

1
2
3
4
5
6
7
8
9
10
11
12
13
14
15
16
17
18
19
20
21
22
23
24
25
26
27
28
29
30
31
32
33
34
35
36
37
38
39
40
41
42
43
44
45
46
47
48
49
50
51
52
53
54
55
56
57
58
59
60

ionization dynamics. Compared to the results obtained by using a simplified model, which takes into account only the elastic reflection of the electrons with constant 0.2 probability at the electrodes, independent of the discharge conditions and surface properties, a completely different electron-power absorption and ionization dynamics are obtained from the simulations with realistic description of the electron-surface interaction. At high voltages we find that energetic ion induced SEs (γ-electrons) cause the generation of a high number of electron induced SEs (δ-electrons) upon impact at one of the electrodes during the time of local sheath collapse. Depending on the instantaneous local sheath voltage these δ-electrons are accelerated into the plasma bulk, generate significant ionization, and can generate electron induced SEE upon impact at the opposing electrode as well. Multiple reflections of both γ- and δ-electrons between the sheaths are observed. These complex non-local dynamics mainly lead to the generation of two beams of energetic electrons at each electrode within an RF period during sheath expansion and collapse, which both propagate into the plasma bulk.

The paper is structured in the following way: in section 2 the model used for the realistic description of the electron-surface interaction in PIC/MCC simulations of CCPs, the input parameters of the model for SiO_2 surfaces, as well as the studied discharge conditions are introduced. The simulation results are presented and discussed in section 3. Finally, conclusions are drawn in section 4.

2. Simulation setup and discharge conditions

The simulations are based on our electrostatic 1d3v Particle-in-Cell code complemented with Monte Carlo treatment of collision processes (PIC/MCC) [34, 35]. Here we investigate geometrically symmetric single-frequency discharges in argon. The distance between the plane, parallel, and infinite electrodes is 6.7 cm. A voltage waveform of $V(t) = V_0 \cos(2\pi f t)$ with $f = 13.56$ MHz is applied to one electrode, while the other electrode is grounded. We assume that the electrodes are made of the same material (SiO_2) and the surface conditions of both electrodes are identical. The neutral gas pressure is 0.5 Pa in all simulations. The gas temperature is constant, taken to be 400 K. The driving voltage amplitude, V_0 is varied between 100 V and 2000 V. Such discharge conditions are typical for plasma etching, sputtering, and PIII. The plasma particles traced in the simulations are electrons and Ar^+ ions. The cross sections for electron-neutral (elastic, ionization, excitation) and ion-neutral (isotropic part of elastic scattering, backward elastic scattering, excitation, ionization) collision processes are taken from [36–38].

We use a realistic model for the description of the electron-surface interaction. In this model the total electron induced SE flux is composed of three components: (i) elastically reflected electrons, (ii) inelastically backscattered electrons, and (iii) electron induced SEs, with emission coefficients η_e, η_i, and δ, respectively. These emission coefficients are determined as proposed by Sydorenko in [39]. First, the empirical formula of

Vaughan [33, 40] is used to approximate the total electron induced SEE coefficient as:

$$\sigma_V = \sigma_{max}[we^{1-w}]^k, \tag{2}$$

where

$$w = \frac{\varepsilon - \varepsilon_0}{\varepsilon_{max} - \varepsilon_0}, \tag{3}$$

$$\sigma_{max} = \sigma_{max,0}\left(1 + \frac{k_s}{2\pi}\theta^2\right), \tag{4}$$

$$\varepsilon_{max} = \varepsilon_{max,0}\left(1 + \frac{k_s}{\pi}\theta^2\right), \tag{5}$$

and

$$k = \begin{cases} 0.56 & \text{if} \quad w < 1, \\ 0.25 & \text{if} \quad w \geq 1. \end{cases}$$

In the above equations ε and θ are the energy and angle of incidence of the PEs ($\theta = 0$ represents normal incidence), ε_0 is the threshold energy for the emission of electron induced SEs, $\varepsilon_{max,0}$ is the energy at the maximum yield and $\sigma_{max,0}$ is the corresponding yield for normal incidence. k is a curve fit parameter, which was determined by Vaughan to fit the results of his model to experimental findings for different surface materials [33, 40]. k_s is a smoothness factor to model the roughness of the surface, its value is between 0 and 2 ($k_s = 0$ for a very rough surface, $k_s = 1$ for a dull surface, and $k_s = 2$ for a polished surface). Via equations (2) - (5) the model takes into account the variation of the electron induced SE yield (and consequently the variation of σ_{max} and ε_{max}) with the energy and angle of incidence as well as with the surface properties.
As a second step, the elastic reflection coefficient, η_e is calculated. At this stage, a correction to the σ_V total emission proposed by Vaughan is introduced by Sydorenko [39]. Here, it is taken into account that about 3 % of the total electron induced SE flux is comprised by elastically reflected electrons at high (several hundreds of eV) PE energies [24], and that there is significant electron emission due to elastic reflection at low (a few tens of eV) PE energies (η_e has a maximum value $\eta_{e,max} \simeq 0.5$ at about $\varepsilon_{e,max} \simeq 5 - 10$ eV [25]). Therefore, η_e is approximated by a function which results in 3 % of the total emission determined by equation (2) at high energies and has a maximum at $\varepsilon_{e,max}$ [39]:

$$\eta_e = r_e\sigma_V + \begin{cases} \eta_{e,max}w_1e^{1-w_1} & \text{if} \quad \varepsilon_{e,0} < \varepsilon < \varepsilon_{e,max} \\ \eta_{e,max}[1 + w_2]e^{-w_2} & \text{if} \quad \varepsilon > \varepsilon_{e,max}, \end{cases} \tag{6}$$

$$w_1 = \frac{\varepsilon - \varepsilon_{e,0}}{\varepsilon_{e,max} - \varepsilon_{e,0}}, \tag{7}$$

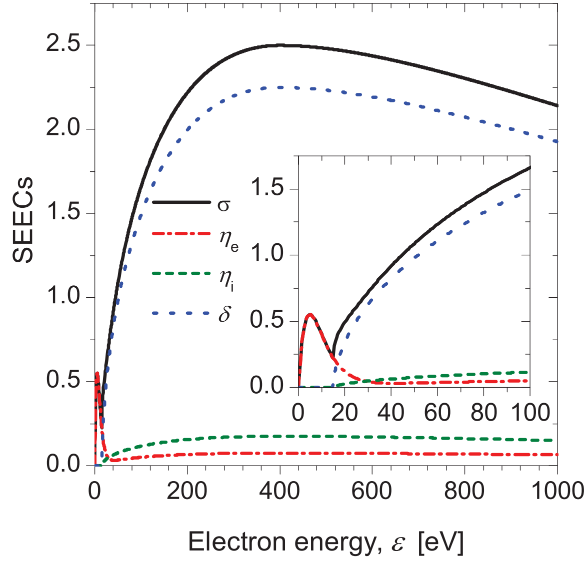

Figure 1. The total electron induced secondary electron emission coefficient (σ) and the partial emission coefficients of the elastic reflection (η_e), inelastic backscattering (η_i), and electron induced secondary electron emission (δ) as a function of the incident electron energy, ε, obtained for normal incidence for SiO_2 surfaces. The parameters of the SEE model are listed in table 1.

$$w_2 = \frac{\varepsilon - \varepsilon_{e,max}}{\Delta_e}, \tag{8}$$

where $\varepsilon_{e,0}$ is the threshold energy for the elastic reflection and Δ_e is a parameter which controls the decay of η_e as a function of ε for electron energies $\varepsilon > \varepsilon_{e,max}$. The r_e parameter, set to 0.03, controls the portion of the elastically reflected electrons of the total electron induced SE flux for high energies. The second term on the right hand side of equation (6) represents the correction to the total emission proposed by Vaughan, σ_V, as in the original model the secondary electron emission vanishes for PE energies $\varepsilon < \varepsilon_0$.

Finally, η_i and δ are determined. The inelastic reflection coefficient, η_i, is calculated as

$$\eta_i = r_i \sigma_V, \tag{9}$$

where the r_i parameter, set to 0.07, reflects that 7 % of the emitted SE flux are inelastically backscattered electrons [24]. The electron induced SEE coefficient, δ is obtained as

$$\delta = (1 - r_e - r_i)\sigma_V. \tag{10}$$

The total emission coefficient, $\sigma = \eta_e + \eta_i + \delta$ equals to σ_V at high energies, while at low energies σ differs from σ_V due to the correction term in eq. (6). Figure 1 shows the total emission coefficient σ and the partial emission coefficients η_e, η_i, and δ obtained by

1
2
3
4
5
6
7
8
9
10
11
12
13
14
15
16
17
18
19
20
21
22
23
24
25
26
27
28
29
30
31
32
33
34
35
36
37
38
39
40
41
42
43
44
45
46
47
48
49
50
51
52
53
54
55
56
57
58
59
60

Table 1. Parameters of the realistic model of the electron-surface processes for SiO_2.

#	Parameter	Description	Value	References
1	ε_0	the threshold energy for electron induced SEE	15 eV	
2	$\varepsilon_{max,0}$	the energy of PE at the maximum emission	400 eV	[23]
3	$\sigma_{max,0}$	the maximum emission at normal incidence	2.5	[23]
4	k_s	smoothness factor of the surface	1	
5	$\varepsilon_{e,0}$	the threshold energy for elastic reflection	0 eV	[41]
6	$\varepsilon_{e,max}$	the energy of PE at the maximum elastic reflection	5 eV	[25]
7	$\eta_{e,max}$	the maximum of the elastic reflection	0.5	[25]
8	Δ_e	control parameter for the decay of η_e	5 eV	[41][a]
9	r_e	portion of elastically reflected electrons	0.03	[24]
10	r_i	portion of inelastically reflected electrons	0.07	[24]

[a] This parameter was determined based on experimental data on the elastic reflection coefficient for dielectrics other than SiO_2 in [41].

using the above formulas for the set of parameters listed in table 1. These parameters were set according to the characteristics of SiO_2 surfaces.

For all discharge conditions we perform simulations by using two different models which operate with different approaches for the description of the electron-surface interaction: (i) model A assumes that the electrons are elastically reflected at the surfaces with a constant probability of 0.2 [42], independently of their energy and angle of incidence, and the other electron-surface processes are completely neglected. This approach is typical in most PIC/MCC simulations of low-pressure CCPs. (ii) model B incorporates the realistic model for the electron-surface interaction presented above, in which the elastic reflection, the inelastic backscattering, and the emission of electron induced true SEs depend on the energy of the incident electron and its angle of incidence. In the simulations we assume SiO_2 electrodes, therefore in model B the parameters of the SEE model are set accordingly (see table 1).

In the simulations a constant ion induced secondary electron emission coefficient of $\gamma = 0.4$ is used for SiO_2 surfaces [43]. We disregard the implementation of an energy-dependent SE yield for ions in this study, since our aim here is to present the impact of taking into account the electron induced SEs on the calculated discharge characteristics. The assumption of a constant γ is clearly a simplification. The combination of the present realistic model for the electron induced SEE with energy-dependent SE yields for heavy particles will be addressed in a future study.

The energy of SEs is uniformly distributed between 0-5 eV for SEs induced by ions, and between 0-20 eV for true SEs induced by electrons, while their angular distribution is isotropic [24, 44]. The inelastically backscattered electrons are emitted with energies uniformly distributed between zero and the incident particle energy, while the elastically reflected electrons (emitted specularly at the surface) have the same energy as the incident electron.

3. Results

Below, we give a comparison between the results obtained from PIC/MCC simulations based on model A (without realistic treatment of electron-surface interactions) and model B (with realistic treatment of electron-surface interactions). Figure 2 shows the ion density in the center of the discharge, n_i^A and n_i^B, respectively, as a function of the driving voltage amplitude, V_0, at $p = 0.5$ Pa, $f = 13.56$ MHz (left vertical scale). In both models the plasma density increases by increasing the driving voltage amplitude. However, in model A n_i^A changes by a factor of about 14 by increasing V_0 from 100 V to 2000 V, whereas in model B n_i^B changes by a factor of about 60 when V_0 is increased from 100 V to 1700 V. By using model A, the simulations converge for the whole domain of driving voltage amplitudes (100 V – 2000 V), while in case of model B $V_0 = 1700$ V is the maximum driving voltage amplitude for which convergence can be obtained. On the right vertical scale of figure 2 the n_i^B/n_i^A ratio of the central ion densities is shown as a function of V_0. At low voltage amplitudes ($V_0 < 300$ V) both models result in similar values for the peak ion density. At high voltage amplitudes, however, a significant difference is found between n_i^A and n_i^B. At $V_0 = 1700$ V $n_i^B/n_i^A = 5$, i.e., a 5 times higher plasma density is obtained from the model which treats the electron-surface interaction in a realistic way (model B) compared to results obtained by using a simplified model for the description of the electron-surface interaction (model A).

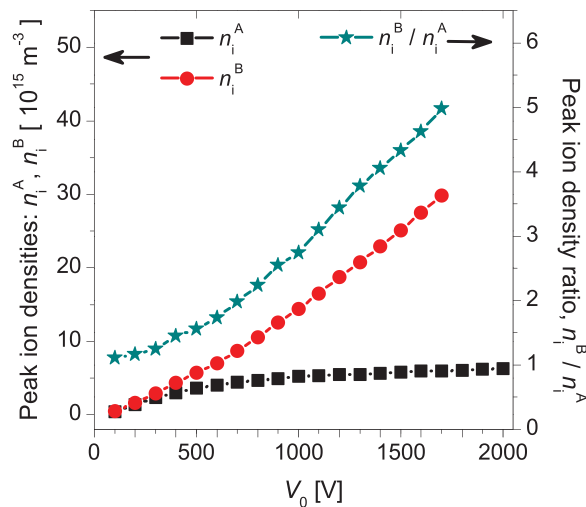

Figure 2. The central ion density obtained from model A and model B, n_i^A and n_i^B (left vertical scale) and the density ratio n_i^B/n_i^A (right vertical scale) as a function of the driving voltage amplitude, V_0. Discharge conditions: argon, SiO_2 electrodes, $L = 6.7$ cm, $p = 0.5$ Pa, $f = 13.56$ MHz, $\gamma = 0.4$.

Figure 3(a) displays the time-averaged charged particle density profiles in the discharge gap, obtained from simulations based on model A and model B for $V_0 = 1000$ V. At this voltage amplitude the ratio of the peak ion densities, n_i^B/n_i^A is about 2.75 (figure 2). Simulation results obtained by assuming perfect absorber surfaces for electrons are

1
2
3
4
5
6
7
8
9
10
11
12
13
14
15
16
17
18
19
20
21
22
23
24
25
26
27
28
29
30
31
32
33
34
35
36
37
38
39
40
41
42
43
44
45
46
47
48
49
50
51
52
53
54
55
56
57
58
59
60

also shown, resulting in maximum charged particle densities of about 3.4×10^{15} m^{-3}. Compared to these results, about 1.5 times higher particle densities are obtained from a simulation based on model A (5.2×10^{15} m^{-3}), while model B results in more than 4 times higher particle densities (14.5×10^{15} m^{-3}) in the discharge center. Besides the differences in the peak charged particle densities, this figure also reveals the significant difference in the sheath length obtained from the different models. The comparison of the results of models A and B for the charged particle density distributions clearly shows that the realistic description of the electron-surface interaction in the model has a strong effect on the calculated discharge characteristics. At higher voltage amplitudes these differences are even more pronounced.

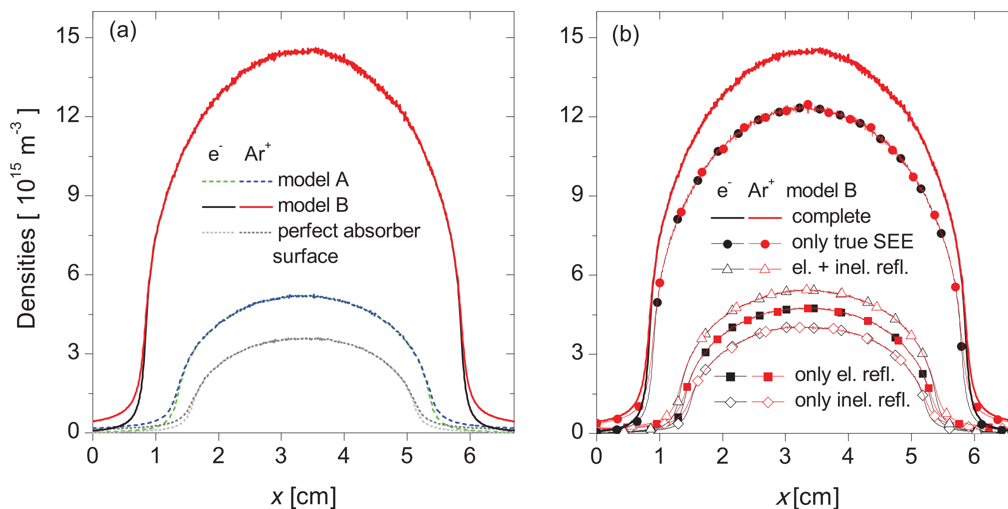

Figure 3. (a) Time-averaged charged particle density distributions obtained from PIC/MCC simulations based on model A (dashed lines) and model B (continuous lines). Results obtained by assuming perfect absorber surfaces for electrons are also included (dotted lines). (b) Time-averaged charged particle density distributions obtained from simulations based on model B by switching on/off the different individual electron-surface processes (elastic reflection, inelastic backscattering, electron induced SEE) in the model. Discharge conditions: argon, SiO_2 electrodes, $L = 6.7$ cm, $p = 0.5$ Pa, $f = 13.56$ MHz, $V_0 = 1000$ V, $\gamma = 0.4$.

Figure 3(b) reveals the importance of the individual electron-surface processes taken into account in model B (elastic reflection, inelastic backscattering, electron induced SEE) in shaping the time-averaged charged particle density distributions based on model B (shown in figure 3(a)) for $V_0 = 1000$ V. These distributions were obtained by switching on/off the individual electron-surface processes in model B: simulations were performed by taking into account only the elastic reflection, only the inelastic backscattering, both of these processes, and only the electron induced SEE. The emission coefficients of these processes were calculated based on equations (1)-(10) for parameters listed in table 1 for SiO_2 surfaces. Figure 3(b) shows the results based on the complete model B as well (the same results are shown in figure 3(a)), where all the three electron-surface

processes were taken into account. The lowest plasma densities are obtained when only the inelastic backscattering or only the elastic reflection is taken into account in the model (4×10^{15} m^{-3} and 4.75×10^{15} m^{-3}, respectively). When both the elastically reflected and inelastically backscattered electrons are taken into account, model B leads to a plasma density of 5.38×10^{15} m^{-3}, which is close to the one obtained from model A (5.2×10^{15} m^{-3}), in which only the elastic reflection of the electrons is taken into account with constant 0.2 probability (see figure 3(a)). A remarkable increase of the charged particle densities and a significant decrease of the sheath length is found when the emission of true SEs induced by electrons is included in the model: the plasma density is 12.4×10^{15} m^{-3} in this case, which is about 85 % of the plasma density obtained from the complete model B. These results indicate that the emission of true SEs induced by electrons is the fundamental process behind the enhanced plasma densities obtained from model B.

In order to understand how the emission of electron induced SEs affects the electron power absorption and ionization dynamics and leads to the drastic change of plasma parameters at high voltage amplitudes in model B compared to model A, the spatio-temporal plots of some selected discharge characteristics are analyzed for $V_0 = 1000$ V. Figure 4 shows the spatio-temporal distributions of the electric field (first row), the electron power absorption (second row), the total ionization rate (third row), and the electron density (fourth row) obtained from model A (left column) and model B (right column) for the same discharge conditions. All panels of figure 4 cover two RF periods on the horizontal axis. The simulation based on model A results in discharge operation in the classical α-mode [45, 46]: the ionization is dominated by the electrons that are accelerated at the expanding sheath edge; one beam of highly energetic electrons is generated at both electrodes during a RF period as the sheath expands, which propagates through the bulk at low pressures and causes ionization (figure 4(e)). Most of these beam electrons hit the opposing sheath during its collapse.

A significantly different ionization dynamics is found in the simulation results based on model B (figure 4(f)). In this case, two beams of energetic electrons, which propagate towards the plasma bulk, are generated at both electrodes during a RF period, and consequently, two separate maxima in the spatio-temporal distribution of the ionization rate can be observed at both electrodes during a RF period (figure 4(f)): (i) strong ionization at the expanding sheath edge (beam I) and (ii) additional ionization during sheath collapse (beam II, weaker compared to beam I). The ionization caused by the energetic electrons of beam I at the expanding sheath edge is much stronger than the ionization in the α-mode observed in the results of model A (figure 4(e)). The beam II of energetic electrons and the related ionization are only present in the results obtained from the complete model B, where, besides the elastic and inelastic backscattering processes, the electron induced SEE is also taken into account. In the results of model B, the generation of an electric field reversal at each electrode during sheath collapse can also be observed (figure 4(b)) [47, 48]. It is caused by the necessity to balance the ion and electron fluxes to each electrode on time average in the presence of strong electron

1
2
3
4
5
6
7
8
9
10
11
12
13
14
15
16
17
18
19
20
21
22
23
24
25
26
27
28
29
30
31
32
33
34
35
36
37
38
39
40
41
42
43
44
45
46
47
48
49
50
51
52
53
54
55
56
57
58
59
60

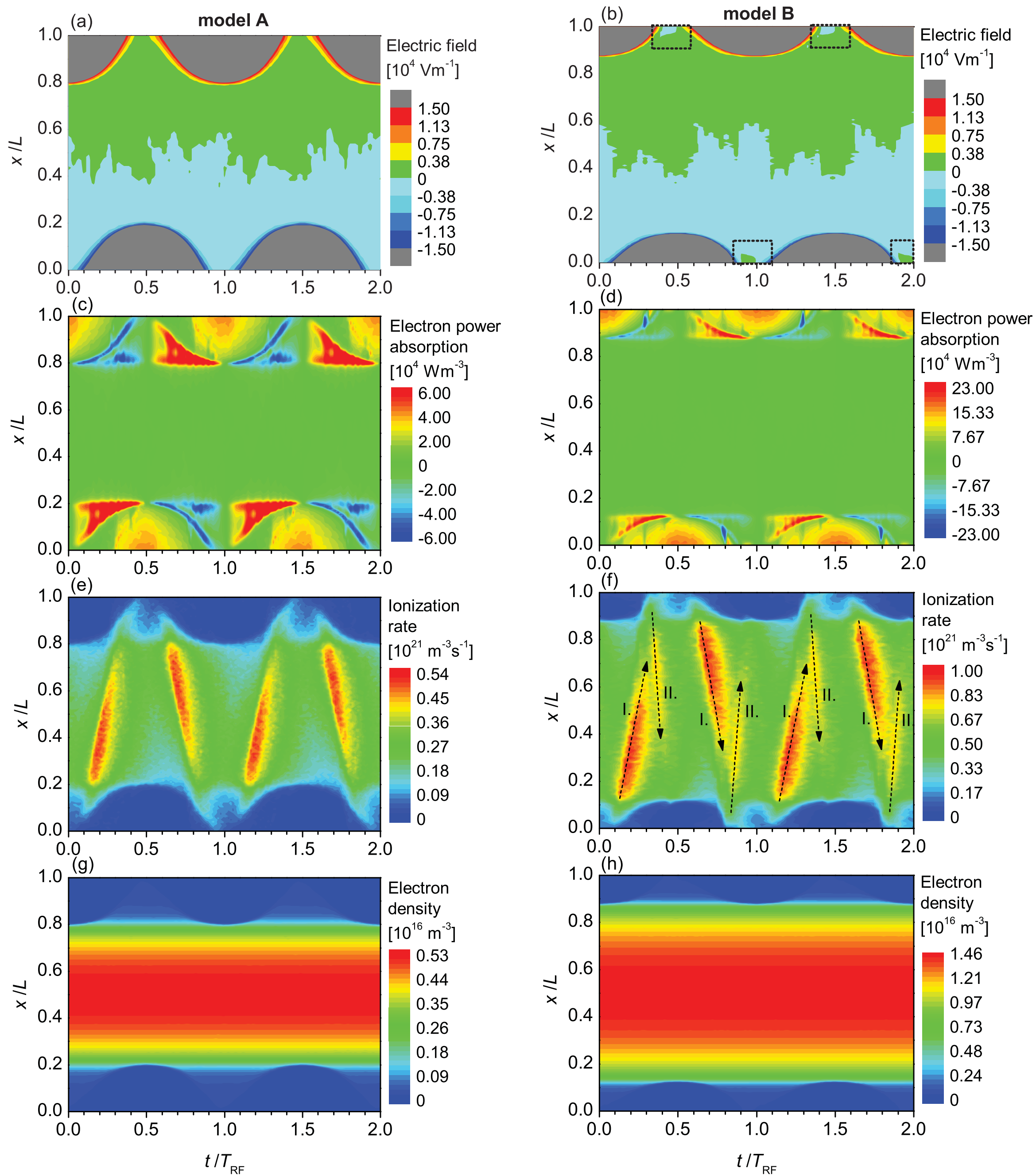

Figure 4. Spatio-temporal distributions of the electric field (first row), the electron power absorption (second row), the total ionization rate (third row), and the electron density (fourth row) obtained from model A (left column) and model B (right column). Discharge conditions: argon, SiO_2 electrodes, $L = 6.7$ cm, $p = 0.5$ Pa, $f = 13.56$ MHz, $V_0 = 1000$ V, $\gamma = 0.4$. The horizontal axis corresponds to two RF periods. The vertical axis shows the normalized distance from the powered to the grounded electrode. The dashed rectangles in panel (b) show the regions of field reversal.

emission from these boundary surfaces. Under these conditions, in order to absorb a sufficiently high number of electrons to compensate the ion flux, a reversed electric field

must be generated to facilitate the electron transport to each electrode during sheath collapse. In this way some of the emitted electrons are pulled back to the surface, where they can be absorbed. This situation is similar to the phenomenon of inversed sheaths in DC discharges, that occurs in the presence of strong electron emission from the boundary surfaces and has been analyzed in detail by Campanell et al. [49, 50].

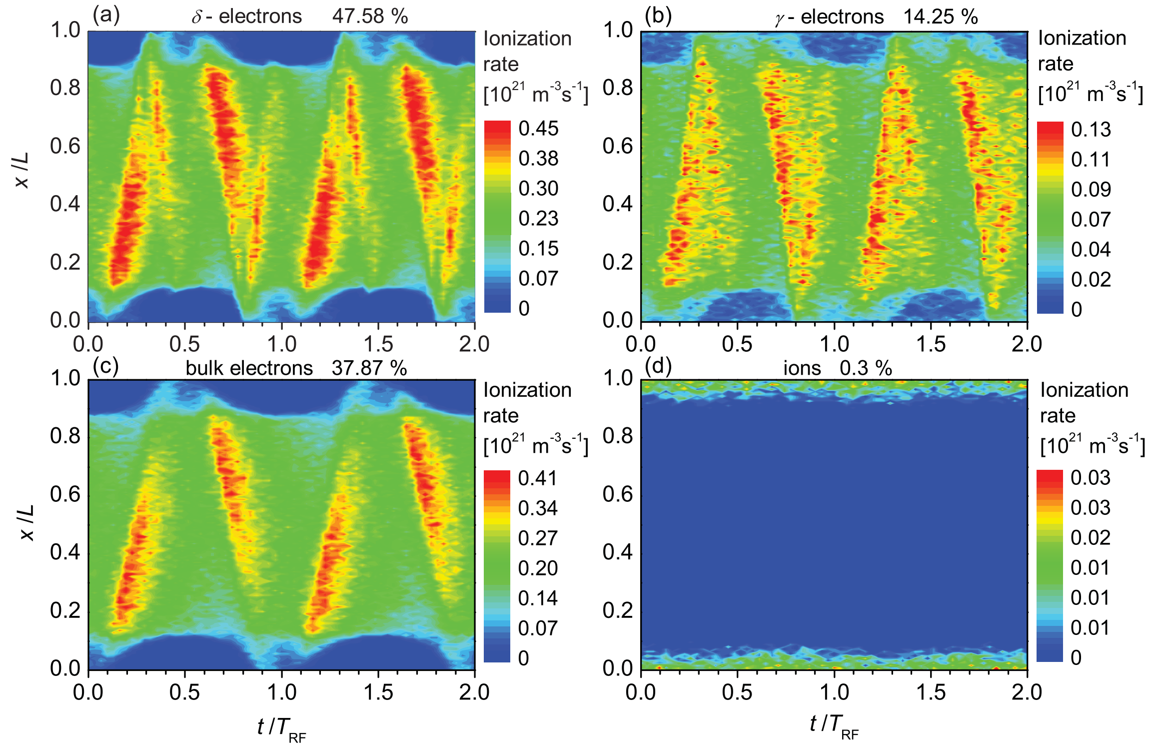

Figure 5. Spatio-temporal plots of the contributions of δ-electrons (a), γ-electrons (b), bulk electrons (c), and ions (d) to the total ionization (shown in figure 4(f)) obtained by using model B. Discharge conditions: argon, SiO_2 electrodes, $L = 6.7$ cm, $p = 0.5$ Pa, $f = 13.56$ MHz, $V_0 = 1000$ V, $\gamma = 0.4$. The horizontal axis corresponds to two RF periods. The vertical axis shows the normalized distance from the powered to the grounded electrode.

Figure 5 shows the individual contributions of δ-electrons (electron induced SEs), γ-electrons (SEs induced by ions), bulk electrons (electrons generated in electron- or ion-impact ionization processes), and ions to the total ionization rate shown in figure 4(f), obtained from simulations based on model B for $V_0 = 1000$ V. Under these conditions the δ-electrons play an important role in the ionization dynamics. The most significant portion of the ionization (48 % of the total) is directly generated by these plasma particles (panel (a)), while the contribution of γ-electrons to the total ionization is 14 % (panel (b)). 38 % of the total ionization is induced by bulk electrons. Ions mostly cause ionization close to the electrodes, however, their contribution to the total ionization remains below 1 % (panel (d)). Figure 5 reveals that the electron beams launched shortly before the sheath collapses at both electrodes (beams II in figure 4(f))

are mainly composed of δ-electrons (figure 5(a)), while the γ-electrons have only a slight contribution to these beams (figure 5(b)). The panels (a) and (b) of figure 5 show that the electrons of beams II are efficiently confined inside the bulk: the δ- and γ-electrons in these beams, launched at one electrode, when the local sheath is partially collapsed, hit the expanded sheath at the opposing electrode, where they are reflected back into the bulk and generate additional ionization. Figure 5(a) also shows that the δ-electrons play a critical role in the α-mode ionization generated at the times of sheath expansion (beams I in figure 4(f)). Their contribution to the ionization at the expanding sheath edges is comparable to the one caused by bulk electrons (figure 5(c)).

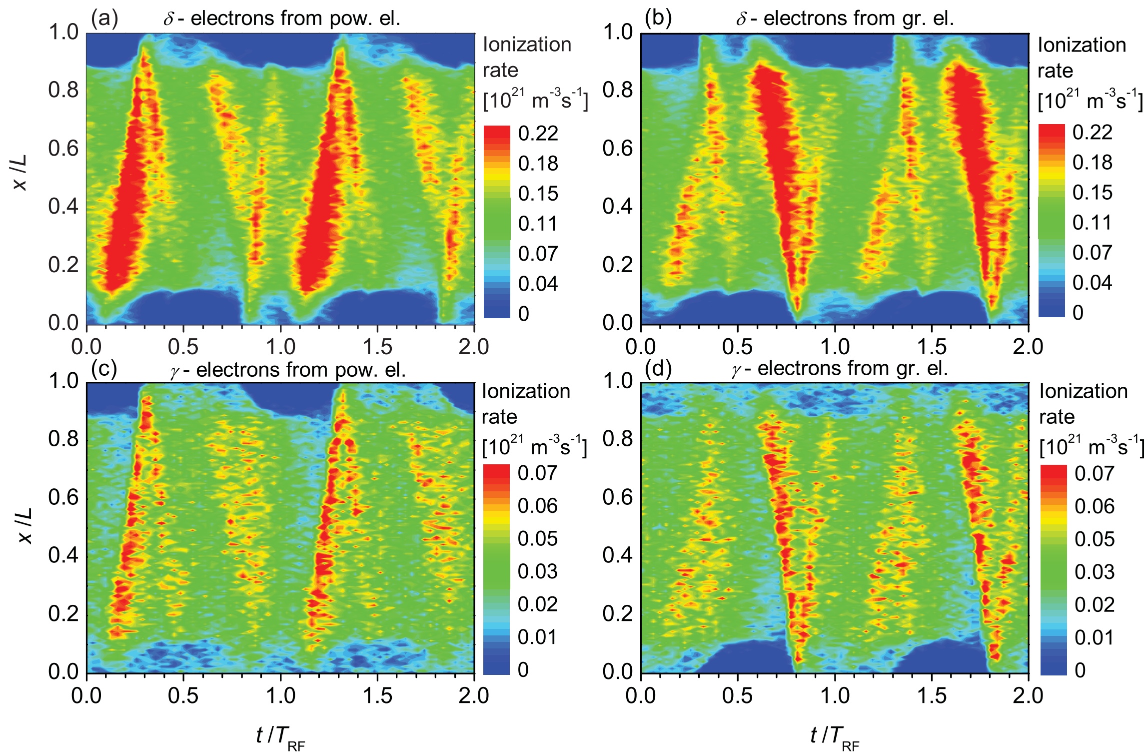

Figure 6. Spatio-temporal plots of the ionization generated by δ-electrons (top row) and γ-electrons (bottom row) emitted at the powered (a,c) and grounded (b,d) electrodes, obtained by using model B. Discharge conditions: argon, SiO_2 electrodes, $L = 6.7$ cm, $p = 0.5$ Pa, $f = 13.56$ MHz, $V_0 = 1000$ V, $\gamma = 0.4$. The horizontal axis corresponds to two RF periods. The vertical axis shows the normalized distance from the powered to the grounded electrode.

The efficient confinement of the electrons in beams II is well visible in figure 6, which shows the ionization induced by δ- and γ-electrons according to their origin: the ionization induced by δ-electrons created at the powered and grounded electrodes are shown in panels (a) and (b), respectively; similarly, the ionization due to γ-electrons created at the powered and grounded electrodes are shown in panels (c) and (d), respectively. Figure 6 provides further insight into the composition of the electron beams II. For instance, the electron beam launched at about $t/T_{\rm RF} = 0.8$ at the

powered electrode (figure 4(f)) is mainly composed of (i) electron induced SEs (δ-electrons) generated at the powered electrode (figure 6(a)), (ii) δ-electrons generated at the grounded electrode which are reflected at the powered electrode sheath (figure 6(b)), and (iii) γ-electrons generated at the grounded electrode which are reflected from the powered electrode sheath also have a slight contribution to this beam (figure 6(d)). Figure 7(a) shows the primary electron flux (IN e^- flux) and the outgoing electron induced SE flux (OUT e^- flux) at the powered (bottom-left axes) and grounded (top-right axes) electrodes. At the powered electrode the electron induced SE flux (which comprises all the three types of electron induced SEs emitted at each electrode) is higher than the flux of incoming PEs at about $0.6 < t/T_{\mathrm{RF}} < 0.9$ and at $1.05 < t/T_{\mathrm{RF}} < 1.3$, which indicates that the emission of electron induced SEs is significant at these phases. This is confirmed in figure 7(b), in which the SE fluxes shown in panel (a) are decomposed, and the flux of reflected electrons (including elastically reflected and inelastically backscattered electrons) is shown separately from the flux of electron induced SEs at both electrodes. The low and constant flux of SEs induced by ion impact is also shown in panel (b).

Now, we discuss the dynamics of the electron-surface interactions, which lead to the ionization dynamics shown in figures 4 - 6. We analyze this dynamics in detail at the powered electrode based on figure 7. The same dynamics happens at the grounded electrode half a RF period later: Within the time interval $0.8 < t/T_{\mathrm{RF}} < 1.3$ figure 7(b) shows a significant emission of true SEs induced by electrons from the powered electrode. During this time interval of sheath collapse at the powered electrode the sheath at the grounded electrode is expanded and γ-electrons generated at the grounded electrode and accelerated by the high instantaneous sheath voltage reach the powered electrode during the local sheath collapse. The energetic γ-electrons from the grounded electrode can overcome the residual sheath potential at the powered electrode within this time interval, hit the electrode at high energies (figure 8(d)), and generate a high number of δ-electrons (figure 7(c)). Before and after this time interval γ-electrons emitted at the grounded electrode cannot reach the powered electrode surfaces, since their energy is too low to overcome the instantaneous local sheath potential. The δ-electrons generated at the powered electrode in this way are accelerated into the bulk by the residual sheath voltage at the powered electrode. The local sheath voltage is only high at the beginning (sheath collapse) and at the end (sheath expansion) of this time interval. Thus, δ-electrons are accelerated to high energies and propagate into the bulk only when the sheath collapses and expands, but not when it is completely collapsed at the powered electrode. A significant fraction of the ionization caused by the two beams of energetic δ-electrons emitted from the powered electrode within one RF period is generated in this way (figure 6(a)). A high number of these δ-electrons reach the opposite sheath at the grounded electrode. Depending on the instantaneous local sheath potential they are either reflected back into the bulk or hit the grounded electrode, where they can induce the emission of new electrons (figure 7(c)). Meanwhile, at the grounded electrode electron induced SEE is also caused by γ-electrons emitted from the

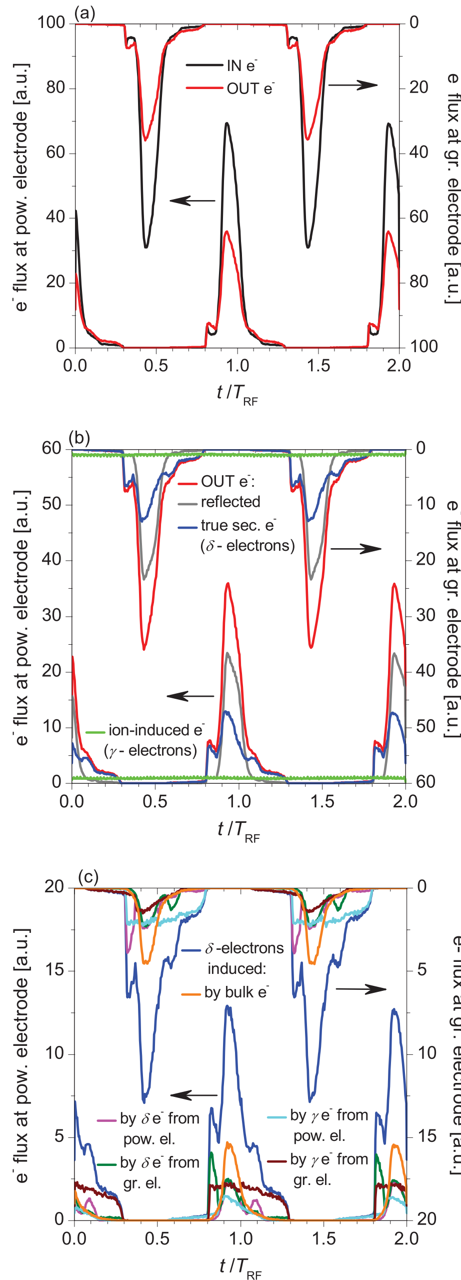

Figure 7. (a) Primary electron flux (IN e$^-$) and electron induced total SE flux (OUT e$^-$) at the powered (bottom-left scale) and grounded (top-right scale) electrodes. IN and OUT are directions relative to the electrode surfaces. (b) Electron induced total SE flux and its components (reflected electrons and true secondary (δ) electrons) at the powered (bottom-left scale) and grounded (top-right scale) electrodes. The flux of ion induced SEs (γ-electrons) is also shown at both electrodes. (c) The outgoing flux of δ-electrons and the contribution of bulk electrons to the electron induced SEE, as well as the contribution of δ-electrons and γ-electrons (emitted at both electrodes) to the SEE. Discharge conditions: argon, SiO_2 electrodes, $L = 6.7$ cm, $p = 0.5$ Pa, $f = 13.56$ MHz, $V_0 = 1000$ V, $\gamma = 0.4$.

powered electrode. We note that while γ-electrons emitted at both electrodes induce less ionization than δ-electrons and bulk electrons (figure 5), they contribute significantly to the production of δ-electrons (figure 7(c)), which dominate the ionization dynamics. All these effects lead to the formation of different groups of energetic secondary electrons that propagate towards the powered electrode and hit this boundary surface at different times around its sheath collapse. Figure 8 shows the mean energy of these different types of electrons at the powered electrode as a function of time together with their fluxes and the flux of outgoing δ-electrons generated by the respective incident electrons. This dynamics leads to the formation of different peaks of the outgoing δ-electron flux at the powered electrode induced by these different groups of incident electrons (figure 7(c)). Amongst other effects this complex dynamics of the electron-surface interactions also leads to contributions of energetic δ-electrons generated at the grounded electrode to the ionization induced by the two beams of energetic electrons that propagate from the powered electrode sheath into the plasma bulk according to figures 4 - 6. When the sheath at the powered electrode is collapsed completely, low energy bulk electrons reach the electrode, cause a high outgoing flux of electrons due to electron reflection (figures 7(b) and 8(e)), and also contribute to the emission of δ-electrons (figure 7(c)).

Overall, the ionization caused by the first electron beam generated during sheath expansion is stronger compared to the ionization generated by the second beam during sheath collapse. This is caused by the presence of stochastic electron heating only during sheath expansion and the good quality of highly energetic electron confinement at the grounded electrode prior to the sheath expansion at the powered electrode. The latter effect ensures that a high number of energetic electrons is reflected at the grounded sheath at this time during the RF period and arrives at the powered electrode during the local sheath expansion phase and, thus, enhances the ionization rate caused by the first electron beam.

Another interesting effect observed in figures 5 and 6 is the fact that ionization by γ-electrons is only observed while one of the sheaths is expanding or collapsing, but not when one of the sheaths is fully expanded. This is significantly different from the classical γ-mode operation of CCPs at high pressures and at low voltages, where maximum ionization is observed at the time of maximum sheath voltage due to the efficient acceleration and collisional multiplication of electrons inside the sheaths [45]. Under the low pressure and high voltage conditions studied here there is only a weak collisional electron multiplication inside the sheaths. At the time of maximum sheath voltage within the RF period γ-electrons are accelerated to extremely high energies up to 1 keV, at which the cross-section for ionization is significantly lower compared to its value at γ-electron energies found during sheath expansion and collapse, when the instantaneous sheath voltage is lower.

Overall, the confinement of energetic electrons is outstandingly important under these low pressure conditions, and the ionization dynamics works significantly differently compared to the α-mode, which is typically assumed to be present under such conditions. In fact, advanced diagnostics such as Phase Resolved Optical Emission Spectroscopy

1
2
3
4
5
6
7
8
9
10
11
12
13
14
15
16
17
18
19
20
21
22
23
24
25
26
27
28
29
30
31
32
33
34
35
36
37
38
39
40
41
42
43
44
45
46
47
48
49
50
51
52
53
54
55
56
57
58
59
60

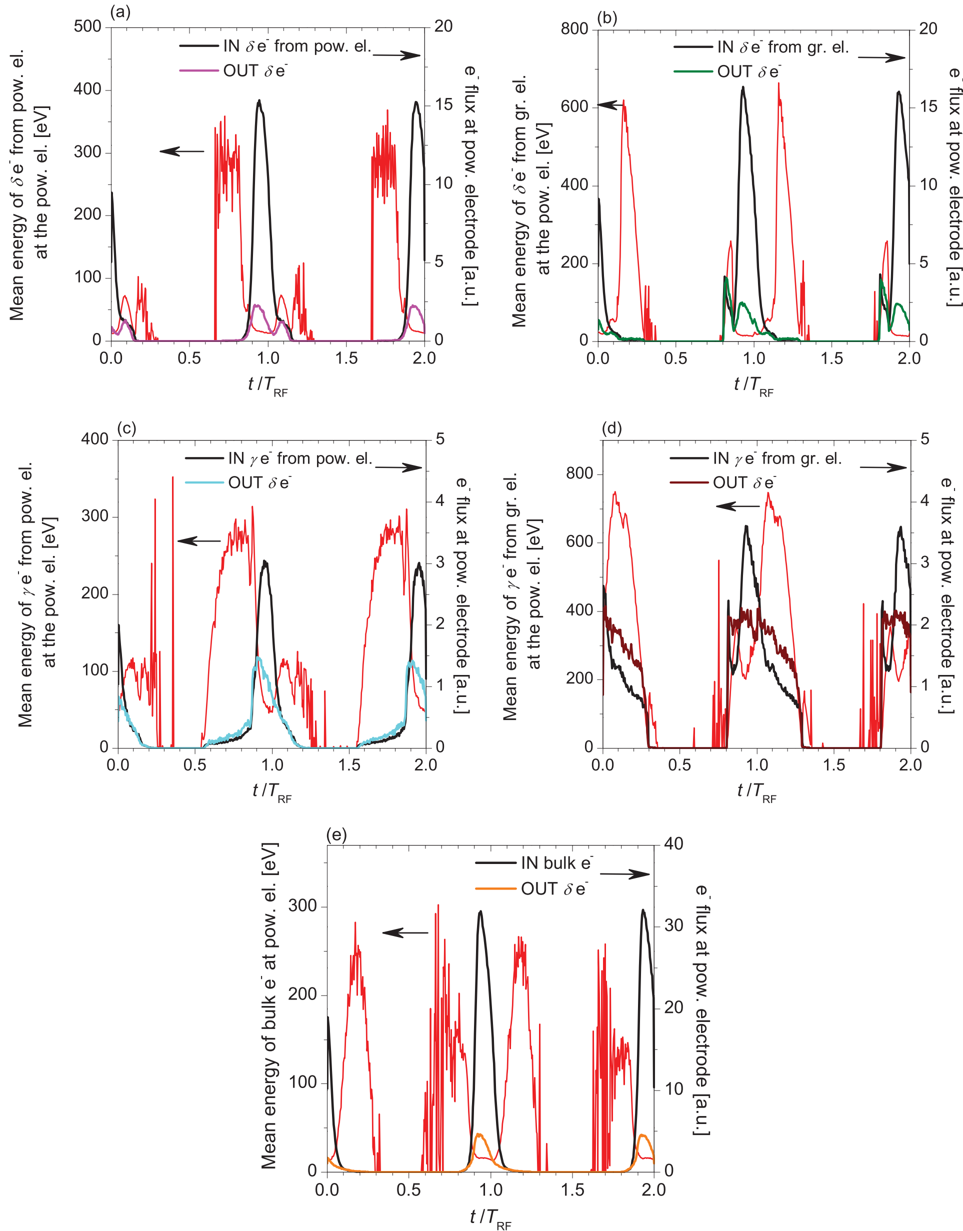

Figure 8. Mean energy (red line, left vertical scale) of different particles (δ-electrons, γ-electrons, bulk electrons), their flux (IN) at the powered electrode, and the flux of true secondary electrons (OUT δ e^-) induced by these particles (right vertical scale). Discharge conditions: argon, SiO_2 electrodes, $d = 6.7$ cm, $p = 0.5$ Pa, $f = 13.56$ MHz, $V_0 = 1000$ V, $\gamma = 0.4$.

(PROES) [51] might indicate α-mode operation, since plasma emission is predominantly observed during sheath expansion. However, as our results show, this can be a false conclusion, depending on the discharge conditions.

4. Conclusions

In this work, we studied the influence of the electron induced SEs (true SEs, δ-electrons) on the electron power absorption and ionization dynamics, and plasma parameters by PIC/MCC simulations in argon gas at a low pressure of 0.5 Pa, for SiO_2 electrodes. The single-frequency discharges were driven at 13.56 MHz, at voltage amplitudes between 100 V and 2000 V. We used a realistic model for the description of the electron-surface interaction. This model takes into account the elastic reflection and the inelastic backscattering of electrons, as well as the emission of electron induced SEs as a function of the energy and angle of incidence of the electrons bombarding the boundary surfaces. The results obtained from this model were compared to those obtained from a simplified model for the electron-surface interaction. In the simplified model, widely used in PIC/MCC simulations of CCPs, only the elastic reflection of electrons at the electrodes is taken into account, with constant 0.2 probability, independent of the discharge conditions and surface properties. A completely different electron power absorption and ionization dynamics were obtained from the two models. The simulations performed by using the realistic model revealed that at low pressures and high voltage amplitudes, the electron induced SEs play a key role in the electron power absorption and ionization dynamics, and largely influence the discharge characteristics.

Their effects on the plasma characteristics were understood by analyzing the spatio-temporal ionization dynamics of the different groups of electrons (δ-, γ-, and bulk-electrons) generated at the powered and grounded electrodes separately. It was found that ion induced γ-electrons generated at one electrode and accelerated to high energies towards the plasma bulk hit the opposite electrode at high energies during the local sheath collapse, whenever they can overcome the local residual sheath voltage. The energetic electron bombardment causes the emission of a high number of δ-electrons, which are accelerated towards the plasma bulk by the residual sheath voltage. These δ-electrons cause significant ionization and propagate through the plasma bulk until they reach the opposite sheath. If they overcome the local sheath voltage, they induce secondary electron emission at this electrode as well. In combination with multiple reflections of energetic δ- and γ-electrons between the sheaths a complex dynamics is formed, which predominantly results in the formation of two beams of energetic electrons at each electrode within a RF cycle, which propagate towards the bulk and cause ionization during the local sheath expansion and collapse phase, respectively.

These results show that the realistic description of the electron-surface interaction is essential at low pressures, especially at high voltage amplitudes, and the emission of true SEs has to be included in discharge models in order to obtain realistic results.

In this work we assumed SiO_2 electrodes in the simulations and set the parameters of the model for the realistic description of the electron-surface interaction accordingly. For SiO_2 surfaces the maximum of the total SEE coefficient was set to 2.5 at 400 eV. The influence of the electron induced SEs on the discharge characteristics is expected to be more pronounced for electrode materials characterized by higher SEE coefficients. The

1 2 3 4 5 6 7 8 9 10 11 12 13 14 15 16 17 18 19 20 21 22 23 24 25 26 27 28 29 30 31 32 33 34 35 36 37 38 39 40 41 42 43 44 45 46 47 48 49 50 51 52 53 54 55 56 57 58 59 60

other discharge parameters, such as pressure, gap length, and driving voltage waveform are also expected to influence the impact of electron induced SEs on the discharge characteristics. These effects will be clarified in a future study.

Acknowledgments

The authors thank Z. Donkó for the useful discussions. This work was supported by the US NSF grant no. 1601080, by the German Research Foundation (DFG) within the frame of the collaborative research centre SFB-TR 87, and by the Hungarian National Research, Development and Innovation Office (NRDI Office) via grants K-119357 and PD-121033.

References

[1] Lieberman M A and Lichtenberg A J 2005 Principles of Plasma Discharges and Materials Processing, 2nd. ed., Wiley Interscience, NJ: Wiley
[2] Makabe T and Petrović Z 2006 Plasma Electronics: Applications in Microelectronic Device Fabrication, Taylor & Francis
[3] Chabert P and Braithwaite N 2011 Physics of Radio-Frequency Plasmas, Cambridge University Press, Cambridge
[4] Birdsall C K and Langdon A B 1985 Plasma Physics via Computer Simulation, New York: McGraw-Hill
[5] Hockney R W and Eastwood J W 1981 Computer Simulation Using Particles, New York: McGraw-Hill
[6] Birdsall C K 1991 *IEEE Trans. Plasma Sci.* **19** 65
[7] Diomede P, Capitelli M, and Longo S 2005 *Plasma Sourc. Sci. Technol.* **14** 459
[8] Matyash K, Schneider R, Taccogna F, Hatazarna A, Longo S, Capitelli M, Tskhakaya D, and Bronold F X 2007 *Contr. Plasma Phys.* **47** 595
[9] Verboncoeur J P 2005 *Plasma Phys. Contr. Fusion* **47** A231
[10] Donkó Z 2011 *Plasma Sourc. Sci. Technol.* **20** 24001
[11] Donkó Z, Schulze J, Hartmann P, Korolov I, Czarnetzki U, Schungel E 2010 *Appl. Phys. Lett.* **97** 081501
[12] Schulze J, Donkó Z, Schuengel E, Czarnetzki U 2011 *Plasma Sourc. Sci. Technol.* **20** 045007
[13] Korolov I, Derzsi A, Donkó Z, Schulze J 2013 *Appl. Phys. Lett.* **103** 064102
[14] Braginsky O, Kovalev A, Lopaev D, Proshina O, Rakhimova T, Vasilieva A, Voloshin D and Zyryanov S 2012 *J. Phys. D.* **45** 015201
[15] Bojarov A, Radmilović-Radjenović M, and Petrović Z Lj 2010 *Proc. 20th ESCAMPIG (13-17 July 2010, Novi Sad, Serbia)* P2.38, Bojarov A, Radmilović-Radjenović M, and Petrović Z Lj 2010, *Publ. Astron. Obs. Belgrade* No. 89 131, Bojarov A, Radmilović-Radjenović M, and Petrović Z Lj 2012 *Proc. 65th Annual Gaseous Electronics Conference (22-26 October 2012, Austin, Texas)*, Bojarov A, Radmilović-Radjenović M, and Petrović Z Lj 2014 *Proc. 27th Summer School and International Symposium on the Physics of Ionized Gases (26-29 August 2014, Belgrade, Serbia)*
[16] Radmilović-Radjenović M and Petrović Z Lj 2009 *Eur. Phys. J. D* **54** 445
[17] Derzsi A, Korolov I, Schüngel E, Donkó Z, Schulze J 2015 *Plasma Sourc. Sci. Technol.* **24** 034002
[18] Hannesdottir H and Gudmundsson J T 2016 *Plasma Sources Sci. Technol.* **25** 055002
[19] Daksha M, Derzsi A, Wilczek S, Trieschmann J, Mussenbrock T, Awakowicz P, Donkó Z, Schulze J 2017 *Plasma Sourc. Sci. Technol.* **26** 085006
[20] Bronold F X and Fehske H 2017 *Plasma Phys. Contr. Fusion* **59** 014011

1 2 3 4 5 6 7 8 9 10 11 12 13 14 15 16 17 18 19 20 21 22 23 24 25 26 27 28 29 30 31 32 33 34 35 36 37 38 39 40 41 42 43 44 45 46 47 48 49 50 51 52 53 54 55 56 57 58 59 60

[21] Bruining H 1954 Physics and Applications of Secondary Electron Emission, Pergamon Press, McGraw-Hill Book Co., New-York

[22] Dekker A J 1958 in Secondary Electron Emission, edited by F. Seitz and D. Turnbull, Solid State Physics Vol 6. (Academic Press, New York) p 251-315

[23] Seiler H 1983 *J. Appl. Phys.* **54** R1–R18

[24] Gopinath V P, Verboncoeur J P, Birdsall C K 1998 *Phys. Plasmas* **5** 1535

[25] Barral S, Makowski K, Peradzynsky Z 2003 *Phys. Plasmas* **10** 4137

[26] Thornton P R 1968 Scanning Electron Microscopy, Applications to Materials and Device Science, Chapman and Hall, London

[27] Gascon N, Dudeck M, Barral S 2003 *Phys. Plasmas* **10** 4123

[28] Sydorenko D, Smolyakovl A, Kaganovich I D, Raitses Y 2006 *Phys. Plasmas* **13** 014501

[29] Kaganovich I D, Raitses Y, Sydorenko D, Smolyakovl A 2007 *Phys. Plasmas* **14** 057104

[30] Taccogna F, Longo S, Capitelli M, Schneider R 2009 *Appl. Phys. Lett.* **94** 251502

[31] Lafleur T, Baalrud S D, Chabert P 2016 *Phys. Plasmas* **23** 053502

[32] Boeuf J-P 2017 *J. Appl. Phys* **121** 011101

[33] Vaughan J R M 1989 *IEEE Transactions on Electron Devices* **36** 1963

[34] Donkó Z 2011 *Plasma Sources Sci. Technol.* **20** 024001

[35] Donkó Z, Schulze J, U Czarnetzki, Derzsi A, Hartmann P, Korolov I, and Schüngel E 2012 *Plasma Phys. Control. Fusion* **54** 124003

[36] Phelps A V *http://jilawww.colorado.edu/∼avp/collision_data/* unpublished

[37] Phelps A V 1994 *J. Appl. Phys.* **76** 747

[38] Phelps A V 1991 *J. Phys. Chem. Ref. Data* **20** 557

[39] Sydorenko D, Particle-in-Cell Simulations of Electron Dynamics in Low Pressure Discharges with Magnetic Fields, PhD thesis (University of Saskatchewan, Saskatoon, Canada, 2006)

[40] Vaughan J R M 1993 *IEEE Transactions on Electron Devices* **40** 830

[41] Bronshtein I M, Fraiman B S: Secondary Electron Emission (Moscow, Russia: Atomizdat, 1969)

[42] Kollath R 1956 *Encyclopedia of Physics* Vol. XXI, ed Flügge S (Berlin, Springer) p 264

[43] Booth J P, Curley G, Maric D, and Chabert P 2010 *Plasma Sourc. Sci. Technol.* **19** 015005

[44] Verboncoeur J P 2005 *Plasma Phys. Control. Fusion* **47** A231

[45] Belenguer P and Boeuf J P 1990 *Phys. Rev. A* **41** 4447

[46] Wilczek S, Trieschmann J, Schulze J, Schuengel E, Brinkmann R P, Derzsi A, Korolov I, Donko Z, Mussenbrock T 2015 *Plasma Sourc. Sci. Technol.* **24** 024002

[47] Schulze J, Donko Z, Heil B G, Luggenhoelscher D, Mussenbrock T, Brinkmann R P, Czarnetzki U 2008 *J. Phys. D* **41** 105214

[48] Czarnetzki U, Luggenhoelscher D, Doebele H F 1999 *Plasma Sourc. Sci. Technol.* **8** 230

[49] Campanell M D, Khrabov A V, Kaganovich I D 2012 *Phys. Rev. Lett.* **108** 255001

[50] Campanell M D 2015 *Phys. of Plasmas* **22** 040702

[51] Schulze J, Schuengel E, Donko Z, Luggenhoelscher D, Czarnetzki U 2010 *J. Phys. D* **43** 124016